



CHORUS

This is the accepted manuscript made available via CHORUS. The article has been published as:

Spin Current Generation Using a Surface Acoustic Wave Generated via Spin-Rotation Coupling

D. Kobayashi, T. Yoshikawa, M. Matsuo, R. Iguchi, S. Maekawa, E. Saitoh, and Y. Nozaki

Phys. Rev. Lett. **119**, 077202 — Published 16 August 2017

DOI: [10.1103/PhysRevLett.119.077202](https://doi.org/10.1103/PhysRevLett.119.077202)

Spin Current Generation Using a Surface Acoustic Wave generated via Spin-Rotation Coupling

D. Kobayashi¹, T. Yoshikawa¹, M. Matsuo^{2,3}, R. Iguchi^{4,5}, S. Maekawa², E. Saitoh^{2,3,5,6}, Y. Nozaki^{1,7}

¹Department of Physics, Keio University, Yokohama, 223-8522, Japan

²Advanced Science Research Center, Japan Atomic Energy Agency, Tokai 319-1195, Japan

³Advanced Institute for Materials Research, Tohoku University, Sendai 980-8577, Japan

⁴National Institute for Materials Science, Tsukuba 305-0047, Japan

⁵Institute for Materials Research, Tohoku University, Sendai 980-8577, Japan

⁶Center for Spintronics Research Network, Tohoku University, Sendai 980-8577, Japan

⁷Center for Spintronics Research Network, Keio University, Yokohama, 223-8522, Japan.

We demonstrate the generation of alternating spin current (SC) via spin-rotation coupling (SRC) using a surface acoustic wave (SAW) in a Cu film. Ferromagnetic resonance caused by injecting SAWs was observed in a Ni-Fe film attached to a Cu film, with the resonance further found to be suppressed through the insertion of a SiO₂ film into the interface. The intensity of the resonance depended on the angle between the wave vector of the SAW and the magnetization of the Ni-Fe film. This angular dependence is explicable in terms of the presence of spin transfer torque from a SC generated via SRC.

The interaction between a localized magnetic moment and spin angular momentum flow, i.e., spin current (SC), has been widely used to control spintronic devices such as spin random access memories [1] and spin-torque oscillators [2]. In general, SC is produced by a nonequilibrium spin state that can be generated using spin accumulation at an interface between ferromagnetic and nonmagnetic materials [3], a thermal gradient in the ferromagnet [4], and phonon [5] or magnon [6] dynamics. Moreover, momentum locking in spins arising from spin-orbital interaction (SOI), which has been widely investigated as the Spin Hall [7] and Rashba [8] Effects, can also be utilized to generate an SC without the use of ferromagnetic materials. It is noted that all of these methods require ferromagnets and/or noble nonmagnetic materials with a strong SOI.

Recently, an alternative method for generating SC in familiar nonmagnetic materials with a weak SOI was theoretically developed by Matsuo et al. based on the coupling between a microscopic spin angular momentum and a macroscopic rotational motion in a nonmagnetic material, i.e., spin-rotation coupling (SRC) [9]. It is widely understood that spin angular momentum can be mutually converted using macroscopic rotation in accordance with the law of angular momentum conservation. Indeed, conversion from a magnetic moment originating in spin angular momentum to macroscopic rotation was experimentally demonstrated in ferromagnetic bodies by Einstein and De Haas [10], while Barnett produced the inverse

conversion [11]. Based on an analytical solution of the Dirac equation with general covariance, Matsuo et al. theoretically predicted that the same type of mutual conversion can be achieved for free electrons in nonmagnetic metals with a weak spin-orbital coupling [12]. They predicted that, unlike that in ferromagnets, the SRC in nonmagnetic materials can lead to spin accumulation originating from the spin angular momentum of conduction electrons. The SRC is defined by the following Hamiltonian: $H_s = -\frac{\hbar}{2}\boldsymbol{\sigma} \cdot \boldsymbol{\Omega}$, where \hbar is the reduced Planck constant, $\boldsymbol{\sigma}$ is the vector of the Pauli matrices, and $\boldsymbol{\Omega}$ is the angular velocity of macroscopic rotation [13]. Unlike the Zeeman interaction, which couples with a magnetic moment originating from the spin angular momentum, the SRC can directly couple with the spin angular momentum itself.

Matsuo et al. theoretically proposed a method to produce SCs in a semi-infinite nonmagnetic metal using a Rayleigh-type surface acoustic wave (R-SAW) via SRC [9, 14]. In the case of an R-SAW with vorticity $\nabla \times v$, $\boldsymbol{\Omega}$ is given by $\boldsymbol{\Omega} = \frac{1}{2}\nabla \times v$, where v is the velocity field of an R-SAW with an amplitude decaying exponentially along the thickness direction. The lattice deformation of the R-SAW, therefore, generates a gradient in $\boldsymbol{\Omega}$, and the SRC directly converts this vorticity to electron spin in the nonmagnetic material. Thus, the vorticity gradient produces a gradient of spin accumulation, which leads to an opposite flow of up and down spins, i.e., a pure SC. SC generation via SRC is a consequence of the generally covariant Dirac theory, although the vorticity gradient seemed to play the same role

with an effective magnetic field gradient in the Stern–Gerlach experiment [15]. According to SRC theory, an R-SAW propagating along the x -axis [9] corresponds to an SC in the depth (z -axis) direction of a semi-infinite nonmagnetic metal that can be approximately represented as:

$$J_s \approx i \frac{\hbar \sigma_0}{2e} \zeta \frac{\omega^3 u_0}{v_t^2} \frac{\sqrt{1-\xi^2}}{\xi} e^{-k_t z + i(kx - \omega t)} \quad (1)$$

for $k_t z \gg 1$, and:

$$J_s \approx i \frac{\hbar \sigma_0}{2e} \zeta \frac{\omega^3 u_0}{v_t^2} \left(1 + \frac{k_t^2 \lambda_s^2}{1 - \xi^2}\right)^{-1/4} k_t z e^{i(kx - \omega t)} \quad (2)$$

for $k_t z \ll 1$, where σ_0 , v_t , k_t , and λ_s are the electrical conductivity, transverse velocity of the sound wave, transverse wave number, and spin diffusion length in the metal, respectively; u_0 and ω are, respectively, the amplitude and frequency of the R-SAW; ζ is a normalization factor representing conversion efficiency between spin and mechanical rotation [16]; and ξ is a constant given by $\xi \approx (0.875 + 1.12\nu)/(1 + \nu)$ with the Poisson ratio ν , and is related to the dispersion relation between ω and k as $\omega = v_t k \xi$. In the R-SAW case, k_t is given by $k_t = k \sqrt{1 - \xi^2}$, where k is the longitudinal wave number. It is noted that the imaginary unit in Eqs. (1) and (2) represents the phase difference of $\pi/2$ between the vorticity of R-SAW and spin current. As shown in Eqs. (1) and (2), an R-SAW with a high frequency will preferably produce a large J_s . It should be noted that the sign of the vorticity is periodically varied along the x -axis; in other words, the amplitude of the consequent SC is temporally varying and

periodically distributed on the plane. These features make it difficult to measure the SC electrically using the inverse Spin Hall Effect, which is generally used to detect SC [17]. Although the generation of SC via R-SAW SRC has not been demonstrated to date, macroscopic rotation without the use of R-SAW has been reported. Chudo and Ono et al. demonstrated the generation of an SRC-derived Barnett field in both nuclear spin systems and rare earth metals in paramagnetic states using a high-speed rotor with rotational frequencies of up to 10 kHz [18]. Takahashi et al. succeeded in detecting SC generated via the vorticity gradient in a mercury flow by measuring the inverse Spin Hall Effect [19]. Using the techniques used to carry out these experiments, however, it is hard to increase the frequency of mechanical rotation to the order of gigahertz (GHz), which, by contrast, is viable in R-SAW experiments. This underlines the usefulness of SC generation via a mechanism such as R-SAW to understand the SRC at GHz frequencies.

In this Letter, we demonstrate the generation of such a non-uniform, alternating SC through measurement of a ferromagnetic resonance (FMR) derived from a spin transfer torque (STT) of the SC in a ferromagnet (FM)/non-magnet (NM) bilayer. Figures 1(a) and 1(b) show schematics of the basic principles underlying our experiment for verifying the creation of non-uniform alternating SC generated by an R-SAW. The NM and FM layers shown in Fig. 1(a) act as source and detector of the SC, respectively. When the R-SAW propagates at the FM/NM bilayer, an alternating SC is generated in the NM and then, spin accumulation is

diffused toward the interface of the FM/NM bilayer, as shown schematically in Fig. 1(a). The alternating SC injected from the NM to the FM imparts an alternating spin-torque onto the magnetization in the FM, as illustrated in Fig. 1(b). If the strength of the external magnetic field H is consistent with the ferromagnetic resonant field at the frequency of the alternating SC, an FMR is excited and energy dissipation occurs in the FM. Although the SC induced by the R-SAW vorticity via SRC produces both positive and negative STTs on the magnetization of the FM, the energy dissipation from the magnetization damping is independent of the sign of torque. Thus, unlike measurement of SC via inverse Spin Hall Effect, the microwave (MW) absorption in the FM owing to the positive and negative SCs is not compensated; as a consequence, as shown schematically in Fig. 1(b), the amplitude of the R-SAW, which can be easily measured using a vector network analyzer (VNA), is suppressed by the energy dissipation of the FMR excitation. Note that a torque on the magnetization is also produced by a magnetostriction effect in the FM and/or by electromagnetic field leakage from the interdigital transducer (IDT) used for exciting the R-SAW [20]. Furthermore, the SRC in the FM produces a Barnett field, which also applies a torque to the magnetization. These influences should therefore be evaluated to confirm the successful generation of SC via R-SAW in the FM/NM bilayer. In this Letter, we confirm that the FMR excitation from the electromagnetic field can be minimized through the suppression of FMR absorption by inserting a nonmagnetic insulator between the FM and NM or completely removing the NM.

We also confirm that the dependence of FMR absorption on the angle between the external magnetic field and the propagating direction of the R-SAW differs substantially from what would be expected in cases in which magnetostriction of the FM is modulated by the R-SAW [20]. Furthermore, the NM thickness dependence of the MW absorption also strongly suggests that the SC is successfully generated via SRC in the NM.

A schematic experimental setup and photomicrograph of the experimental device used in the study are shown in Fig. 1(c) [21]. The two transducers, IDT1 and IDT2 in Fig. 1(c), perform, respectively, as a transmitter and detector of the R-SAW. As schematically shown in Fig. 1(c), a rectangle of ferromagnetic Ni₈₁Fe₁₉/nonmagnetic Cu bilayer was deposited between the IDTs. Copper was used as a SC generator in our device since, as can be seen from Eqs. (1) and (2), highly conductive materials with a long spin-flip time are favorable for improving SRC. The Ni₈₁Fe₁₉ alloy (hereafter referred to as Py) was used as the FM to reduce the influence of magnetostriction [22]. As shown in Fig. 1(c), the amplitude of the R-SAW propagating from IDT1 to IDT2 was evaluated from VNA measurement of the S_{21} parameter in frequency-domain mode at a given external magnetic field [23]. The MW input power was fixed at -5 dBm because the SRC effect was scaled with the power [24]. An external magnetic field was applied to match the FMR frequency of the FM with the R-SAW frequency. To study the angular dependence of FMR absorption, the angle θ between the external magnetic field and the propagating direction of the R-SAW was adjusted from 0 to

90° at intervals of 10°. For comparison, the same experiment was performed using a sample comprising a rectangle of Py (20 nm) or Py (20 nm)/SiO₂ (20 nm)/Cu (200 nm). All measurements were performed at room temperature, and Ti (5 nm) was deposited as an adhesion layer in all samples.

Figure 2(a) shows a color plot of the reduced MW absorption $\Delta P^{\text{norm}}(f, H)$, given by

$$\Delta P^{\text{norm}}(f, H) = \frac{P_{21}(f, H) - P_{21}(f, H_{\text{ref}})}{P_{SAW}^{\text{peak}}(H_{\text{ref}})} \quad (3)$$

in the rectangular Py(20 nm)/Cu(200 nm) bilayer as a function of frequency and external magnetic field applied along $\theta = 0$. Here $P_{21}(f, H)$ is the transmitted MW power calculated from S_{21} at a given frequency f and an external magnetic field H . $P_{21}(f, H_{\text{ref}})$ represents a reference signal at a given f and fixed magnetic field $\mu_0 H_{\text{ref}} = -15$ mT that is sufficiently large to saturate the magnetization of Py. Note that FMR does not occur at H_{ref} in the frequency range shown in Fig. 2(a). By subtracting $P_{21}(f, H_{\text{ref}})$ from $P_{21}(f, H)$, the field independent signals can be successfully removed and the subtracted P_{21} can be further normalized to $P_{SAW}^{\text{peak}}(H_{\text{ref}})$, which is the peak intensity of $P_{21}(f, H_{\text{ref}})$. The deformation amplitude u_0 of the R-SAW owing to mismatch of acoustic impedance depends on both the material properties between the IDTs and the film thickness. Note that $\Delta P^{\text{norm}}(f, H)$ in Eq. (3) is independent of u_0 because both $P_{SAW}^{\text{peak}}(H_{\text{ref}})$ and the absorption caused by the SRC of the R-SAW, $P_{21}(f, H) - P_{21}(f, H_{\text{ref}})$, are proportional to u_0^2 [25].

When the wave vector of R-SAW is parallel to the magnetization, a magneto-static backward

volume wave (MSBVW) whose wave vector also parallel to the magnetization is expected to be excited. The pair of broken lines in Fig. 2(a) show the dispersion relation of the MSBVW given by

$$f = \frac{|\gamma|}{2\pi} \sqrt{H \left(H + \frac{M_s}{\mu_0} \frac{1 - e^{-kd}}{kd} \right)}, \quad (4)$$

where γ is the gyromagnetic ratio, d is the thickness of FM, k is the wave number of MSBVW and $M_s = 0.98$ T is the saturation magnetization of Py [26]. The vertical dotted line in Fig. 2(a) shows the excitation frequency of the fundamental R-SAW shown in Fig. 2(b), which has a frequency-dependent transmission power. The peak frequency of 1.59 GHz in Fig. 2(b) corresponds to the fundamental frequency of an R-SAW propagating from IDT1 to IDT2 through the rectangular Py/Cu bilayer. As shown in Fig. 2(a), a high degree of MW absorption occurs when the external magnetic field is consistent with the resonant field at the R-SAW excitation frequency; this suggests that the MW absorption is attributable to the interaction between the magnetization and the R-SAW. Figure 2(c) shows an enlarged plot of the FMR absorption in the Py/Cu bilayer occurring when the FMR frequency is matched with the fundamental frequency of the R-SAW. The FMR absorption completely disappeared when time gating was performed in the range of 0 to 100 ns, a time interval preceding the arrival of the R-SAW at IDT2; by contrast, a much faster electromagnetic wave (EMW) reached IDT2 within 100 ns. These results suggest that the FMR excitation arising from EMW propagation from IDT1 to IDT2 was negligibly small. Indeed, as shown in Fig. 2(d), there was little MW

absorption in the Py sample between IDT1 and IDT2. Furthermore, as shown in Fig. 2(e), insertion of insulating SiO₂(20 nm) between the Py and Cu layers also led to strong FMR-based suppression of MW absorption. Together, these results suggest that the presence of both the nonmagnetic Cu layer and the clean interface between the Py and Cu layers are significant to the appearance of the FMR excitation in the Py layer; i.e., as shown schematically in Figs. 1(a) and 1(b), it seems reasonable to suppose that an alternating SC is generated in the Cu layer via SRC, with the subsequent STT leading to FMR excitation in the Py layer. Namely, the Barnett field inside the FM is considered to be very small.

To support the hypothesis of alternating SC generation via SRC in the NM, we examined the angular dependence of FMR absorption in the Py/Cu bilayer. The STT amplitude will be at a maximum when the spin angular momentum of the SC is orthogonal to the magnetization; conversely, a collinear orientation of injected spin with respect to the magnetization will completely eliminate the STT. In the case of SC generated by an R-SAW, the spin angular momentum is oriented along the R-SAW vorticity vector, which lies in a plane orthogonal to the R-SAW wave vector. Thus, the STT strength can be modulated by varying the angle θ between the Ni₈₁Fe₁₉ magnetization and the wave vector of the R-SAW. Figure 3(a) shows the θ -dependence of the peak intensity of MW absorption in the Py/Cu bilayer. The strongest MW absorption is observed at around $\theta = 0$, where a maximum STT would be expected because it is the orientation at which the spin angular momentum of the

SC is orthogonal to the magnetization. The MW absorption monotonously decreases with increasing $|\theta|$. The angular dependence differs entirely from the magnetostriction-dominant case [20]. A comparison of these two R-SAW attenuation cases leads to the conclusion that the angular dependence of MW absorption seen in Fig. 3(a) is attributable to the STT arising from the SC generated by the SRC in the R-SAW.

Finally, the t_{Cu} -dependence of the MW attenuation was examined to check the depth profile of the amplitude of SC generated by the R-SAW SRC, as shown in Fig. 3(b). It was found that the peak amplitude of MW attenuation showed a monotonous increase until 200 nm with increasing t_{Cu} , suggesting that the amplitude of the SC generated by the R-SAW SRC can be improved by increasing t_{Cu} . This is consistent with the theoretically expected depth profile of the spin current. Figure 3(c) shows a numerically evaluated snapshot of the temporal variation in the depth profile of J_s , which is calculated from the gradient of the spin accumulation as obtained by numerical integration of Eq. (9) in Ref. 9. The depth profile of J_s reveals that the maximum amplitude of SC under R-SAW excitation in a semi-infinite nonmagnetic metal is located at $z = 0.79k_t^{-1}$. In the case of Cu with a Poisson constant of 0.343 [27], k_t is evaluated as $1.32 \times 10^6 \text{ m}^{-1}$, which is 0.35 times the wavenumber of the R-SAW [28]. Finally, we can confirm that the depth of maximum J_s is approximately 600 nm from the surface of the metallic film. The monotonous increase in the amplitude of MW absorption until $t_{\text{Cu}} = 200$ nm, as seen in Fig. 3(b), is qualitatively consistent with the theory showing a gradual increase

of SC at the sub- μm scale.

In summary, we demonstrated the conversion of alternating SC from a macroscopic rotation generated by an R-SAW propagating in a Py/Cu bilayer deposited on a LiNbO₃ substrate. An FMR excited in the Ni₈₁Fe₁₉ layer was successfully observed when the fundamental frequency of the R-SAW matched the FMR frequency. The strength of FMR excitation was strongly suppressed when the Cu layer was removed from the bilayer or when an insulating SiO₂ layer was inserted into the interface of the bilayer, presenting clear evidence that the alternating SC generated in the Cu layer via SRC plays an important role in the FMR excitation. The angular dependence of the strength of FMR excitation quantitatively supports the successful generation of alternating SC using the SRC arising from an R-SAW. We further found that the amplitude of SC can be increased by increasing the thickness of Cu layer to 200 nm, which agrees with theoretical expectation. Our experimental results open pathways to the generation of alternating SC in SAW devices without the use of ferromagnets and/or nonmagnetic materials with large SOI.

The authors thank Y. Ohnuma for valuable discussions and comments. This work was supported by JSPS Core-to-Core Program and JSPS KAKENHI Grant Number 17H05183, 15H01021 and 15K05153, and JST ERATO “Spin Quantum Rectification” (JPMJER1402).

Figure captions

Fig. 1 Schematic illustrations of (a) SC generation via SRC in R-SAW and (b) MW absorption owing to FMR excitation caused by SC injection. The R-SAW in Ni₈₁Fe₁₉/Cu bilayer generates a mechanical rotation, which leads to an alternating pure SC in the Cu layer. When the SC is injected into the Ni₈₁Fe₁₉ layer, a spin transfer torque is exerted on the magnetization and an FMR is excited. Some of the elastic energy of the R-SAW is used to excite the FMR, which in turn suppresses the amplitude of R-SAW deformation. (c) Schematic experimental setup for measuring MW absorption caused by the FMR excitation shown in Fig. 1(b). A Ni₈₁Fe₁₉/Cu bilayer was deposited between a pair of IDTs fabricated on a LiNbO₃ piezoelectric substrate. The S_{21} MW transmission coefficient was measured while applying a static magnetic field at an angle θ from the propagating direction of the R-SAW. The inset shows an optical photograph of the device.

Fig. 2 (a) Color plot of reduced MW absorption owing to FMR excitation as a function of frequency and magnetic field at $\theta = 0$ measured for rectangular Py (20 nm)/Cu (200 nm) sample. (b) P_{21} as a function of frequency measured at $\mu_0 H_{\text{ref}} = 40$ mT, where the FMR frequency of the Ni₈₁Fe₁₉ film is much higher than 3 GHz. Enlarged color plots of FMR absorption (top panel) and MW transmission properties (bottom panel) measured for (b) Py (20 nm)/Cu (200 nm), (c) Py (20 nm) and (d) Py (20 nm)/SiO₂ (20 nm)/Cu (200 nm)

rectangular samples fabricated between IDTs.

Fig. 3 (a) Angular dependence of the peak value of normalized MW absorption in Py (20 nm)/Cu (200 nm) rectangle. (b) Cu thickness dependence of the peak value of normalized MW absorption in a Py (20 nm)/Cu (200 nm) rectangle. (c) Numerically evaluated snapshot of the temporal variation in the depth profile of the spin current J_s . The value of J_s is obtained by calculating the gradient of spin accumulation using the analytical expression given by Eq. (9) in Ref. 9.

- [1] H. Ohno, T. Endoh, T. Hanyu, N. Kasai, and S. Ikeda, IEDM Tech. Dig. 218 (2010); M. Hosomi, H. Yamagishi, T. Yamamoto, K. Bessho, Y. Higo, K. Yamane, H. Yamada, M. Shoji, H. Hachino, C. Fukumoto, H. Nagao, and H. Kano, IEDM Tech. Dig. 459 (2005); T. Kishi, H. Yoda, T. Kai, T. Nagase, E. Kitagawa, M. Yoshikawa, K. Nishiyama, T. Daibou, M. Nagamine, M. Amano, S. Takahashi, M. Nakayama, N. Shimomura, H. Aikawa, S. Ikegawa, S. Yuasa, K. Yakushiji, H. Kubota, A. Fukushima, M. Oogane, T. Miyazaki, and K. Ando, IEDM Tech. Dig. 309 (2008); S. Ikeda, J. Hayakawa, Y. M. Lee, F. Matsukura, Y. Ohno, T. Hanyu, and H. Ohno, IEEE Trans. Electron Devices, **54**, 991 (2007); S. Matsunaga, J. Hayakawa, S. Ikeda, K. Miura, H. Hasegawa, T. Endoh, H. Ohno, and T. Hanyu, Appl. Phys. Express, **1**, 091301 (2008).
- [2] S. Kiselev, J. Sankey, I. Krivorotov, N. Emley, R. Schoelkopf, R. Buhrman, and D. Ralph, Nature (London) **425**, 380 (2003); W. H. Rippard, M. R. Pufall, S. Kaka, S. E. Russek, and T. J. Silva, Phys. Rev. Lett. **92**, 027201 (2004); J. A. Katine and E. E. Fullerton, J. Magn. Magn. Mater. **320**, 1217 (2008).
- [3] F. J. Jedema, A. T. Filip, and B. J. van Wees, Nature (London) **410**, 345 (2001).
- [4] K. Uchida, S. Takahashi, K. Harii, J. Ieda, W. Koshibae, K. Ando, S. Maekawa, and E. Saitoh, Nature (London) **455**, 778 (2008).
- [5] K. Uchida, H. Adachi, T. An, T. Ota, M. Toda, B. Hillebrands, S. Maekawa, and E. Saitoh, Nat. Mater. **10**, 737 (2011); K. Uchida, T. An, K. Kajiwara, M. Toda, and E. Saitoh, Appl.

- Phys. Lett. **99**, 212501 (2011); K. Uchida, H. Adachi, T. An, H. Nakayama, M. Toda, B. Hillebrands, S. Maekawa, and E. Saitoh, J. Appl. Phys. **111**, 053903 (2012).
- [6] E. Saitoh, M. Ueda, H. Miyajima, and G. Tatara, Appl. Phys. Lett. **88**, 182509 (2006).
- [7] Y. K. Kato, R. C. Myers, A. C. Gossard, and D. D. Awschalom, Science **306**, 1910 (2004); J. Wunderlich, B. Kaestner, J. Sinova, and T. Jungwirth, Phys. Rev. Lett. **94**, 047204 (2005); T. Kimura, Y. Otani, T. Sato, S. Takahashi, and S. Maekawa, *ibid.* **98**, 156601 (2007).
- [8] J. C. Rojas Sánchez, L. Vila, G. Desfonds, S. Gambarelli, J. P. Attané, J. M. De Teresa, C. Magén, and A. Fert, Nat. Commun. **4**, 2944 (2013); K. Shen, G. Vignale, and R. Raimondi, Phys. Rev. Lett. **112**, 096601 (2014).
- [9] M. Matsuo, J. Ieda, K. Harii, E. Saitoh, S. Maekawa, Phys. Rev. B **87**, 180402 (2013).
- [10] A. Einstein and W. J. de Haas, Experimenteller Nachweis der Ampereschen Molekularströme, Deutsche Physikalische Gesellschaft, Verhandlungen 17, pp. 152–170 (1915).
- [11] S. J. Barnett, Phys. Rev. **6**, 239 (1915).
- [12] M. Matsuo, J. Ieda, S. Maekawa, Phys. Rev. B **87**, 115301(2013).
- [13] C. G. de Oliverira and J. Tiomno, Nuovo Cimento **24**, 672 (1962); B. Mashhoon, Phys. Rev. Lett. **61**, 2639 (1988); J. Anandan, *ibid.* **68**, 3809 (1992); B. Mashhoon, *ibid.* **68**, 3812 (1992); F. W. Hehl and W.-T. Ni, Phys. Rev. D **42**, 2045 (1990).
- [14] J. Ieda, M. Matsuo, S. Maekawa, Solid State Commun. **198**, 52 (2014).

[15] W. Gerlach and O. Stern, *Zeitschrift für Physik*. **8**, 110 (1922); W. Gerlach and O. Stern, *Zeitschrift für Physik*. **9**, 349 (1922); W. Gerlach and O. Stern, *Zeitschrift für Physik*. **9**, 353 (1922).

[16] M. Matsuo, Y. Ohnuma, and S. Maekawa, *Phys. Rev. Lett.* **96**, 020401(R) (2017).

[17] M. I. Dyakonov and V. I. Perel, *Phys. Lett. A* **35**, 459 (1971); J. E. Hirsch, *Phys. Rev. Lett.* **83**, 1834 (1999).

[18] H. Chudo, M. Ono, K. Harii, M. Matsuo, J. Ieda, R. Haruki, S. Okayasu, S. Maekawa, H. Yasuoka, and E. Saitoh, *Appl. Phys. Express* **7**, 063004 (2014); H. Chudo, K. Harii, M. Matsuo, J. Ieda, M. Ono, S. Maekawa, and E. Saitoh, *J. Phys. Soc. Jpn.* **84**, 043601 (2015); M. Ono, H. Chudo, K. Harii, S. Okayasu, M. Matsuo, J. Ieda, R. Takahashi, S. Maekawa, and E. Saitoh, *Phys. Rev. B* **92**, 174424 (2015); Y. Ogata, H. Chudo, M. Ono, K. Harii, M. Matsuo, S. Maekawa, and E. Saitoh, *Appl. Phys. Lett.* **110**, 072409 (2017).

[19] R. Takahashi, M. Ono, K. Harii, H. Chudo, S. Okayasu, M. Matsuo, J. Ieda, S. Takahashi, S. Maekawa, and E. Saitoh, *Nature Phys.* **12**, 52 (2015).

[20] L. Dreher, M. Weiler, M. Pernpeintner, H. Huebl, R. Gross, M. S. Brandt, and S. T. B. Goennenwein, *Phys. Rev. B* **86**, 134415 (2012).

[21] See Supplemental Material [url] for the detail of sample preparation, which includes Ref. [29].

[22] Q. Yang, P. Holody, S.-F. Lee, L. L. Henry, R. Loloee, P. A. Schroeder, W. P. Pratt, Jr.,

and J. Bass, Phys. Rev. Lett. **72**, 3274 (1994).

[23] See Supplemental Material [url] for signal processing process in SRC-FMR experiment, which includes Refs. [30, 31].

[24] See Supplemental Material [url] for scaling of SRC effect with an amplitude of R-SAW.

[25] W. Robbins, IEEE Tran. Sonics and Ultrasonics **24**, 339 (1977).

[26] C. Kittel, Phys. Rev. **73**, 155 (1948).

[27] G. W. Kaye and T. H. Laby, *Tables of physical and chemical constants 16th edition*, (National Physical Laboratory, London, 1995).

[28] See Supplemental Material [url] for estimation of R-SAW wavelength in the Py/Cu metallic bilayer.

[29] K. Shibayama, K. Yamanouchi, H. Sato and T. Meguro, Proc. IEEE **64**, 595(1976).

[30] L. D. Landau and E. M. Lifshitz, *Theory of Elasticity* (Pergamon, New York, 1959).

[31] H. F. Tiersten, J. Appl. Phys., **40**, 770 (1969).

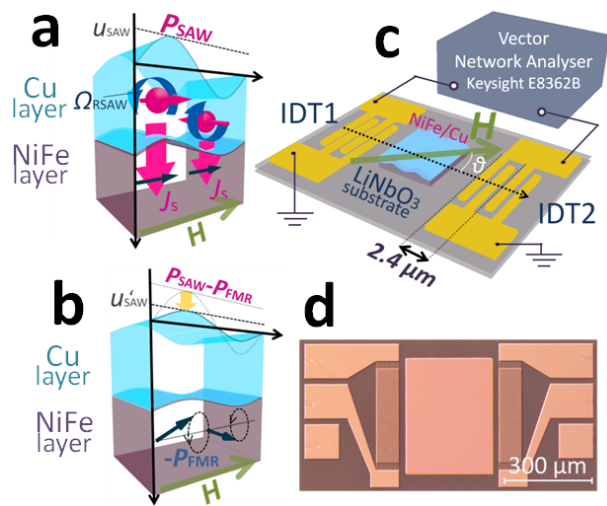


Fig. 1 (Kobayashi et al. submitted to PRL)

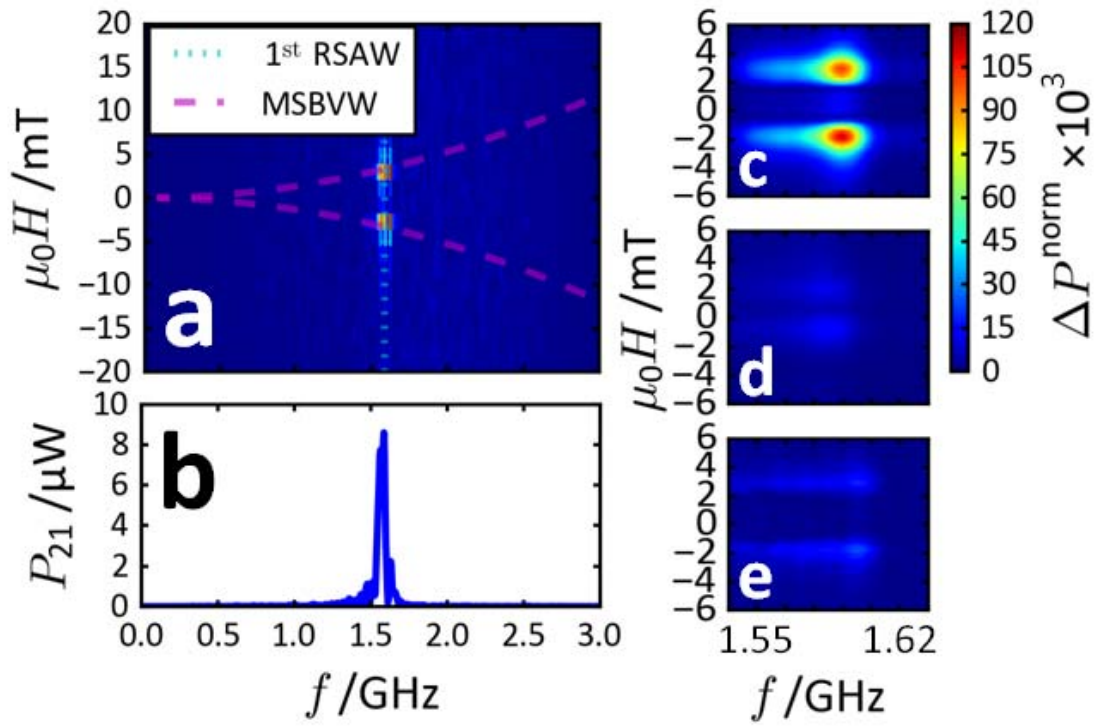


Fig. 2 (Kobayashi et al., submitted to PRL)

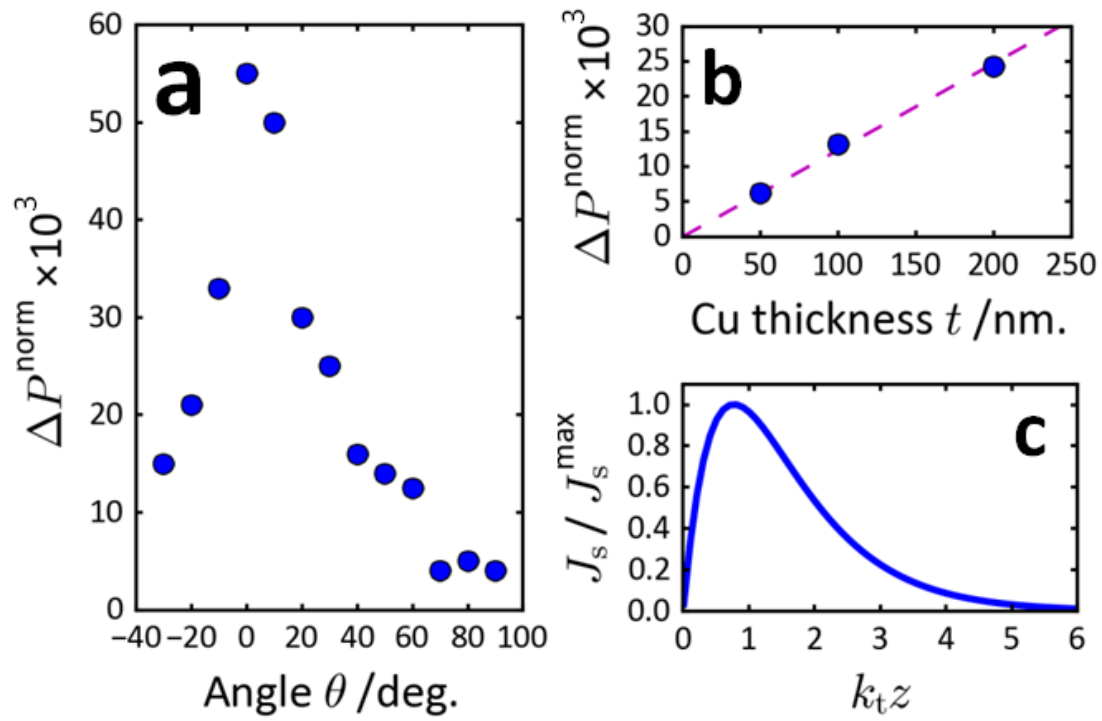


Fig. 3 (Kobayashi et al., submitted to PRL)